Highlights

Bias in modeled solar radiation by non-resolved intra-daily AOD variability

José A. Ruiz-Arias

- Non-resolved intra-daily AOD variability induces a bias in the modeled solar radiation.
- A mathematical formulation is proposed to describe and predict this bias.
- Mean biases of about -0.2 W/m^2 and -2 W/m^2 are found in the global horizontal and direct normal solar irradiances at the surface, respectively.

Bias in modeled solar radiation by non-resolved intra-daily AOD variability

José A. Ruiz-Arias[a,b,*]

[a]*Department of Applied Physics I, University of Málaga, Málaga, Spain.*
[b]*Solargis s.r.o., Bratislava, Slovakia.*

Abstract

Attenuation of broadband solar irradiance by aerosols has been traditionally evaluated in wide areas using aerosol optical depth (AOD) discretized at monthly time steps. This fact is known to induce a bias in the long-term solar irradiance evaluations. Nowadays weather models allow for a spatially-continuous description of AOD at sub-daily steps (e.g., hourly or 3-hourly). But considering the still high uncertainty of their modeled AODs in relation with the natural sub-daily AOD variability, a key question is whether the attenuation of solar irradiance by aerosols could simply be accounted for from daily AOD means. Hence, the bias induced by the non-resolved sub-daily AOD variability should be investigated. This work proposes a mathematical methodology to understand the roots of such a biasformulation and uses AOD observations from 213 ground sites to investigate it. Overall, the mean and standard deviation of the bias at evaluating the daily mean global horizontal solar irradiance stay at about -0.2 and 1.2 W/m^2, respectively, or -2.0

*Corresponding author
Email addresses: jararias@uma.es (José A. Ruiz-Arias), jose.ruiz-arias@solargis.com (José A. Ruiz-Arias)

and 5.5 W/m^2 for direct normal irradiance. The mean of the daily bias nearly vanishes using the proposed methodology while the standard deviation reduces to only 1.0 (3.3) W/m^2 in global horizontal (direct normal) solar irradiance.
Keywords: solar radiation evaluation, aerosol variability, estimation bias, mathematical model

1. Introduction

Atmospheric aerosols play a key role in a multitude of processes that overall rule the course of weather. Most importantly, they act as condensation nucleii in cloud-formation processes and attenuate the long-wave and solar radiation fluxes that traverse the atmosphere. In absence of clouds, aerosols are the main attenuating atmospheric constituent.

Aerosol optical depth (AOD), the main optical parameter to evaluate the extinction of solar radiation by aerosols, is being monitored worldwide from satellite-borne spectroradiometers such as the MODerate resolution Imaging Spectroradiometer (MODIS) and the Multi-angle Imaging SpectroRadiometer (MISR) (Kaufman et al., 2000; Diner et al., 2001) and ground-based sunphotometer networks such as the Aerosol Robotic Network (AERONET; **?**). Nonetheless, the spatially-gridded AOD that is obtained is prone to data gaps because the sensors are typically mounted on polar-orbiting satellites and the AOD retrieval algorithms are valid only under cloud-free situations (Levy et al., 2007, 2013; Ruiz-Arias et al., 2013a). Although gap-filling methods have been proposed (Ruiz-Arias et al., 2013b; Yang and Hu, 2018), the most widely-used approach, by far, is the upscaling of AOD retrievals

to monthly time steps (Levy et al., 2009; De Leeuw et al., 2015). Nowadays, however, atmospheric models coupled with chemistry transport models (Benedetti et al., 2018; Gelaro et al., 2017; Inness et al., 2019; Schulz and Kinne, 2009) provide a comprehensive description of the entire atmospheric aerosol cycle throughout multi-year continuous three-dimensional grids at sub-daily time steps (e.g., 3-hourly or finer) from which aerosol databases and climatologies are produced, most often, over monthly time grids (Kinne et al., 2013; Zubler et al., 2011). These data bases are used to evaluate the solar resource amount (Gueymard and Sengupta, 2013; Ruiz-Arias and Gueymard, 2018a,b), the global radiative energy budget (Hinkelman, 2019; Wild et al., 2015) or as initial and boundary conditions in subsequent numerical weather simulations (Bozzo et al., 2017).

As shown by Ruiz-Arias et al. (2016a,b,c), the global horizontal irradiance (GHI) and the direct normal irradiance (DNI) under cloud-free situations are underestimated by up to about 2 % and 10 %, respectively, when a monthly time grid, instead of daily, is used to describe AOD. The reason is the loss of variability when AOD is represented only at monthly time steps. This systematic underestimation, accumulated throughout time in scales of weeks to months or longer, may also result in non-negligible forcings in numerical simulations of weather (Benedetti and Vitart, 2018) and in biases in the evaluated solar resource amount. Hence, a sub-daily or, at least, daily AOD from atmospheric models should be preferred in the evaluation of the solar radiation amount at the surface. However, although model simulations can generally reproduce the aerosol large-scale circulation, the uncertainty of their AOD predictions is still greater than the actual intra-daily variability of AOD

(Kocha et al., 2013; Smirnov et al., 2002). Hence, it is not clear that modeled AODs can faithfully reproduce the sub-daily variability of AOD. For instance, Inness et al. (2019) has shown that the standard deviation of the differences between modeled AOD at 550 nm in the brand new Copernicus Atmosphere Monitoring Service reanalysis (CAMS) and observations at more than 900 AERONET sites is 0.11. However, according to the AERONET data set described in Section 3.1, which encompasses 203617 site-days throughout 213 AERONET sites, the mean intra-daily standard deviation of AOD at 550 nm is only 0.03, with 90 % of the days having intra-daily standard deviations lower or equal than 0.07. This fact seems to discourage the use of sub-daily modeled AOD values in favor of daily averages at evaluating the solar radiation amount at the surface. Nonetheless, disregarding the AOD sub-daily variability by using daily or coarser AOD representations induces a bias that depends on the non-resolved AOD variability. Depending on the application, this bias might be important, particularly in those that involve or are affected by long-term evaluations of solar radiation.

For illustration purposes, Fig. 1 shows the diurnal profiles of simulated clear-sky GHI and DNI with the SMARTS radiative transfer model (described in Section 3.2) at the Izaña AERONET station (Canary Islands, Spain) for two days that have, respectively, low and high variability of Angström turbidity, β (i.e., AOD at 1 μm). In order to highlight the impact of neglecting the sub-daily variability of AOD, the diurnal profiles of GHI and DNI are calculated for two variations of the input dataset: (i) directly using the observations of β and precipitable water, w, registered at the AERONET station (hereinafter also referred to as reference case), and (ii) assuming β

and w stay constant throughout the day to their respective observed daily mean values. For reasons that will become clear later, the sub-daily variations of w are also considered in this evaluation. The Angström exponent, α, is assumed constant and equal to its observed daily mean value such that only the impacts of β and w variations on the calculated clear-sky GHI and DNI are considered. However, note that the effect of the variability of α in this illustration case is expected very low because it stays fairly constant and similar during the two days (0.20 and 0.18). Note also that its value shows that coarse aerosols, presumably from maritime and desert origin as it is expected at Izaña, are dominating during both days.

At first sight, one might expect that the daily mean clear-sky GHI and DNI values (shown in parenthesis in the plot legends) obtained using the actual β and w observations (reference case) and using their respective daily mean values were nearly undistinguishable because the diurnal period during which clear-sky solar irradiance is underestimated is counterbalanced by the period during which it is overestimated. This reasoning appears to be supported by Fig. 1a, in which both the diurnal profiles and daily mean values of simulated clear-sky GHI and DNI are nearly alike both in the reference case and when daily mean values of β and w are considered. Indeed, the daily mean clear-sky DNI in the latter case is only 1 W/m^2 below the reference case. For GHI, the difference is even lower (0.5 W/m^2). However, Fig. 1b shows larger differences not only in the diurnal profiles of clear-sky GHI and DNI but also in their daily mean values (the daily mean clear-sky DNI considering constant β and w values is 10.8 W/m^2 below the reference case and is 1 W/m^2 below in the case of GHI). This day displays a much higher variabil-

ity of both β and w, which is presumably produced by an intrusion of humid air (possibly also dust) starting before noon. This increased variability of β, and also w to some extend, explains the biases in the modeled GHI and DNI with respect to the reference case as it will be described in Section 2.

This work quantifies the bias that underlies the simulation of GHI and DNI under cloud free situations when AOD is accounted for using daily averages instead of instantaneous values. To that aim, an observational data set that includes spectral AOD and precipitable water observations from 213 AERONET sites spanning the period 2000-2018 is used and a general mathematical framework is formulated to demonstrate that this bias depends on a combination of both the non-resolved intra-daily AOD variability and the transfer of solar radiation throughout the atmosphere. Furthermore, it is shown that this formulation allows to predict the bias from the daily AOD mean and variance (i.e., without any sub-daily description of AOD) and a solar radiation model that describes the radiative transfer of the atmosphere.

2. Mathematical framework

Let AOD be the random variable τ with mean μ_τ and variance σ_τ^2. In our working context, they are, respectively, the AOD mean and variance values throughout a day. (Hereinafter, μ_x and σ_x^2 are used to denote, respectively, the mean and variance of a variable x). Let R be the physical radiative transfer model that evaluates the solar irradiance at the surface (i.e., for this discussion, it interchangeably evaluates GHI and DNI). For simplicity, let's by now assume that R only depends on τ. If the sub-daily changes of τ are neglected, thus considering τ is fixed to a constant value μ_τ throughout

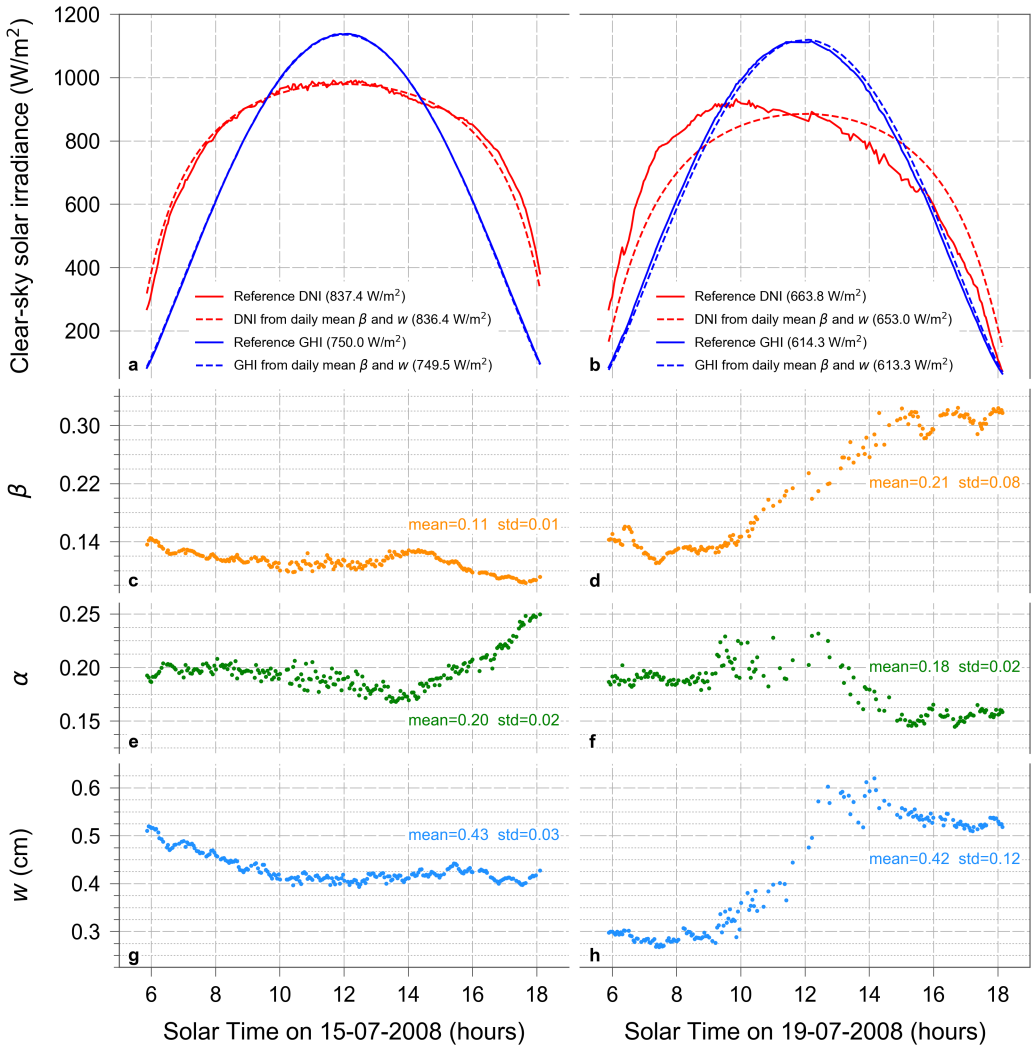

Figure 1: Diurnal profiles of simulated clear-sky GHI and DNI (panels a and b), and observed Angström turbidity (β; panels c and d), Angström exponent (α; panels e and f) and precipitable water (w; panels g and h) at the Izaña AERONET station (Canary Islands, Spain) for two days with low β and w variability (left column) and high β and w variability (right column). The clear-sky solar irradiance simulations are performed with the SMARTS radiative transfer model (described in Section 3.2) for two variations of the input dataset: using direct observations of β and w (reference case; panels c–h) and assuming they are constant throughout the day to their respective daily mean values (shown in panels c–h together with the daily standard deviation, std). The daily mean values of simulated clear-sky GHI and DNI are shown in parenthesis in panels a and b.

the entire day, it might be argued that the actual daily mean R, μ_R, can be simply evaluated as $R(\mu_\tau)$. The potential difference between $R(\mu_\tau)$ and μ_R is the bias underlying the evaluation of R using daily mean τ instead of the actual sub-daily values. This work hinges upon this estimation bias. Hereinafter, $R(\mu_\tau)$ is referred to as *zero-order* approximation.

The actual mean solar irradiance at the surface is defined as

$$\mu_R = \int_0^{+\infty} R(\tau)P(\tau)d\tau, \tag{1}$$

where $P(\tau)$ is the probability density function of τ such that $\int_0^{+\infty} P(\tau)d\tau = 1$.

The value of $R(\tau)$ in the neighborhood of μ_τ can be evaluated with a Taylor expansion series as follows:

$$R(\tau) = R(\mu_\tau) + \sum_{n=1}^{+\infty} \frac{1}{n!} \frac{d^n R}{d\tau^n}\bigg|_{\mu_\tau} (\tau - \mu_\tau)^n, \tag{2}$$

where the first term of the right-hand side is the zero-order approximation and the following are higher-order Taylor correction terms. Note that the derivatives are all evaluated at μ_τ.

Combining Eq. (1) and (2), μ_R can be evaluated as:

$$\mu_R = R(\mu_\tau) + \sum_{n=1}^{+\infty} \frac{1}{n!} \frac{d^n R}{d\tau^n}\bigg|_{\mu_\tau} M_n(\tau), \tag{3}$$

where

$$M_n(\tau) = \int_0^{+\infty} (\tau - \mu_\tau)^n P(\tau)d\tau \tag{4}$$

is the n-order central moment of $P(\tau)$. Equation (3) shows that, in general, the zero-order approximation $R(\mu_\tau)$ is different from μ_R. Thus a bias in the latter is expected when it is approximated only by the former. This is the

case when daily (monthly) mean solar irradiance is evaluated from the daily (monthly) mean AOD.

Since the first-order central moment is zero, the second-order central moment is the variance of $P(\tau)$ and furthermore neglecting the higher-order Taylor correction terms, Eq. (3) reduces to:

$$\mu_R \approx R(\mu_\tau) + \frac{1}{2}\frac{d^2R}{d\tau^2}\bigg|_{\mu_\tau} \sigma_\tau^2. \tag{5}$$

Therefore, $R(\mu_\tau)$ reduces to μ_R only when: (i) τ is constant (i.e., $\sigma_\tau^2 = 0$) or, (ii) the radiative transfer model is linear (i.e., $\frac{d^2R}{d\tau^2} = 0$). Indeed, in the latter case, $R(\tau) = a + b\tau$ for arbitrary parameters a and b independent of τ. Then, $\mu_R = \overline{R(\tau)} = \overline{(a + b\tau)} = a + b\mu_\tau = R(\mu_\tau)$, as it is also predicted by Eq. (5).

Hence, considering that the radiative transfer of the atmosphere is a non-linear process, estimating the solar irradiance at the surface throughout a day only from the zero-order approximation generally results in a systematic error approximated by the second term of the right-hand side of Eq. (5), hereinafter referred to as *second-order* approximation. A simple case example is that of DNI, which is computed as the product of the short-wave atmospheric transmittances by every constituent of the atmosphere. Since atmospheric transmittance is a decaying exponential (Bohren and Clothiaux, 2006), its second derivative is always positive and Eq. (5) predicts that $R(\mu_\tau)$ is always smaller than μ_R because $\sigma_\tau^2 > 0$ necessarily. This is consistent with the results obtained by Ruiz-Arias et al. (2016a,b,c) purely based on data analysis using Monte Carlo methods.

In the more general case, R not only depends on τ but also on solar position and other atmospheric constituents. By assuming that R depends

on m independent variables x_i, it can be demonstrated that Eq. (5) extends to:

$$\mu_R \approx R(\vec{\mu}) + \frac{1}{2}\sum_{i=1}^{m} \left.\frac{\partial^2 R}{\partial x_i^2}\right|_{\vec{\mu}} \sigma_i^2, \tag{6}$$

where $\vec{\mu} = (\mu_1, \mu_2, ..., \mu_m)$, with μ_i and σ_i^2 being, respectively, the mean and variance of variable x_i. The first and second terms of the right-hand side are the generalization of the zero- and second-order approximations, respectively.

The second-order approximation provides a mathematical foundation to explain why and how a bias appears when sub-daily AOD variability is neglected. A thorough investigation of higher-order Taylor correction terms is postpone for future analyses.

3. Data and methods

3.1. Ground observations

The observational data set comprises AOD at multiple wavelengths and precipitable water observations from the All-points Level-2 AERONET data base, Version 3, (Giles et al., 2019) at 213 sites spanning the period 2000–2018. The observations are gathered typically every 15 min although those observations affected by clouds are screened during the AERONET's quality control check. Although the uncertainty in the AOD measurements can be highly variable, **?** Only days with 30 or more final observations with solar altitude greater than 10° are retained in order to guarantee a representative sampling of AOD throughout each day, overall totaling 203617 site-days at all sites combined. (The term site day specifically refers to the fact that the AERONET observations gathered at any two different sites during the same day are treated independently and count as two different "site day"

instances.) The mean period covered by the observations within the day is of 8.7 hours and for 90 % of the site days this time lapse is higher or equal than 6.9 hours. The sites are classified by rough prevailing aerosol type into fine, mixed or coarse aerosol class following the clustering approach described in Ruiz-Arias et al. (2016a). This classification scheme results in 108 fine, 68 mixed and 37 coarse aerosol sites with 97427, 71611 and 34579 site days, respectively. Broadly speaking, the fine aerosol sites are mostly affected by anthropogenic aerosols and biomass burning, whereas the coarse aerosol sites are mostly affected by sea salt and dust.

Fig. 2 shows the AERONET sites locations and aerosol prevailing type (Fig. 2a) as well as the data distribution of Angström turbidity (Fig. 2b) and precipitable water (Fig. 2c) by means of boxplots. Overall, the coarse sites present the highest AOD turbidity and mean daily variability. The latter is a consequence of the wider dynamic range of AOD values. At coarse sites, precipitable water is also slightly higher than at mixed and fine aerosol sites.

3.2. Radiative transfer modeling and data pre-processing

The Simple Model of the Atmospheric Radiative Transfer of Sunshine (SMARTS) spectral radiative transfer model (Gueymard, 2019) is used to simulate GHI and DNI (i.e., it is used as a surrogate of the function R introduced in Section 2). SMARTS is an accurate clear-sky parametric model extensively used in a broad range of fields such as the atmospheric sciences, solar resource assessment and forecasting or solar energy technologies, among others (see Gueymard, 2019, and references therein). It simulates the solar spectrum from 0.28 to 4.0 μm at 2002 wavelengths and has demonstrated an outstanding performance at simulating clear-sky broadband fluxes compared

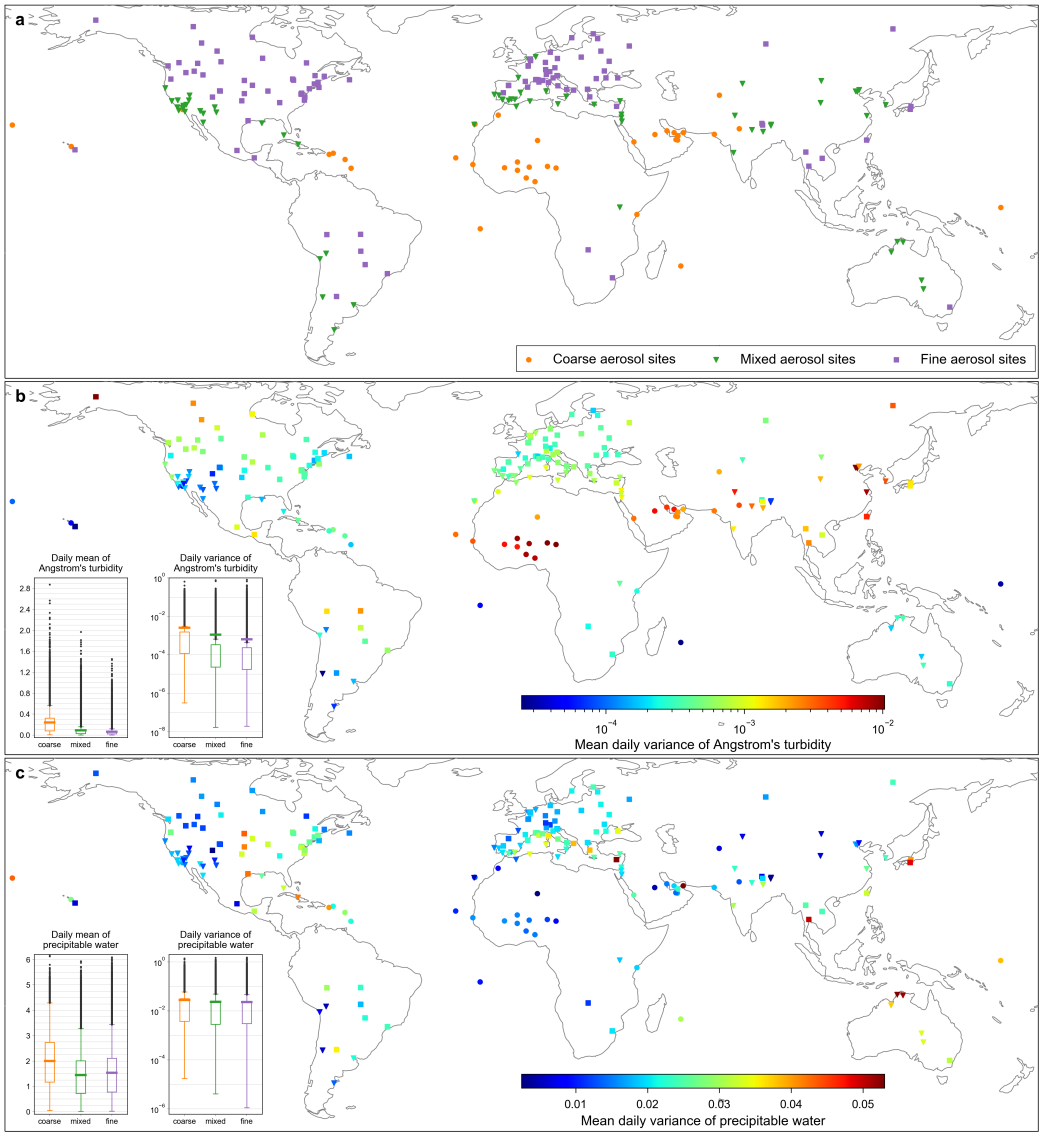

Figure 2: Location of the AERONET sites used in this study and mean properties at each site during the period 2000–2018: (a) prevailing aerosol type, (b) mean daily variance of β and (c) mean daily variance of w. The insets in panels b and c show boxplots of the daily mean and variance of β and w, respectively, by aerosol type at all sites combined. The boxplot boxes enclose the inter-quartile range (i.e, from first to third quartiles) and the whiskers extend one inter-quartile range beyond the box limits. The gray dots are observations beyond the whiskers limits and the thick horizontal lines on or near the boxes mark the mean value of each dataset.

to rigorous physical models and ground observations (Ruiz-Arias et al., 2013c; Ruiz-Arias and Gueymard, 2018a).

SMARTS simulates aerosol scattering and absorption from the Angström turbidity and the Angström exponent. The latter is obtained after a *log-log* fit of the AOD measurements between 440 and 870 nm following the Angström's formula (Eck et al., 1999). It is directly available in the AERONET data set (variable *440-870_Angstrom_Exponent*). However, Angström turbidity is not directly observed so that it is here extrapolated from the observed AOD at 1020 nm using the Angström's formula and the AERONET's retrieved α. When AOD at 1020 nm is not available, the closer spectral channel available below 1 μm (e.g., AOD at 870 nm) is used to perform the extrapolation to 1 μm. To simulate the attenuation by water vapor, SMARTS requires precipitable water, which is directly available in the AERONET data set (variable *Precipitable_Water(cm)*).

Since, in general, the impact of α on R is of lower importance than that of β and w, the impact of the intra-daily variability of α is deemed negligible with respect to that of β and w and all the calculations with SMARTS are performed using the mean Angström exponent, μ_α, observed each day. This is and approximation that may have an impact in the results, although it is expected low, and can however largely simplify the interpretation of results. Notwithstanding, part of the impact of α is already accounted for because the data set is stratified by prevailing aerosol conditions, which are tightly related to α. In parallel, since (in general) the impact of w on R cannot be neglected against that of β, the effect of the sub-daily variability of both β and w is jointly investigated using Eq. (6) as it is described in Section 3.3.

Default values are used for the rest of input parameters required by SMARTS, namely: total column ozone (0.3 cm), surface albedo (0.2), aerosol single-scattering albedo (0.92) and aerosol asymmetry parameter (0.7). Atmospheric pressure is calculated from each site's altitude using the hypsometric equation with a scale-height parameter of 8434 m above mean sea level.

In summary, the radiative transfer simulations with SMARTS are driven by sub-daily changes of β, w and solar zenith angle as well as daily changes in α, keeping fixed the rest of input parameters. In what follows, only these four variables are therefore explicitly considered as input drivers of SMARTS.

3.3. Simulation of daily solar irradiances

At every sub-daily i-th time slot of the j-th day in the observational data set, SMARTS is run with the observed Angström turbidity, β_i^j, precipitable water, w_i^j, and daily mean Angström exponent, μ_α^j, and the calculated solar zenith angle, $\theta_{z,i}^j$. The subsequent GHI and DNI outputs are averaged as follows:

$$\mu_R^j = \frac{1}{N_j} \sum_{i=1}^{N_j} R\left(\theta_{z,i^j}, \beta_i^j, w_i^j; \mu_\alpha^j\right), \tag{7}$$

where μ_R^j and N_j are the daily mean solar irradiance R (GHI or DNI) and the number of observations, respectively, for the j-th day. Subsequently, the model is run similarly for each j-th day with daily mean Angström turbidity, μ_β^j, and daily mean precipitable water, μ_w^j, to estimate the zero-order approximation of daily mean solar radiation, $\hat{\mu}_{R,0}^j$, as:

$$\hat{\mu}_{R,0}^j = \frac{1 N_j \sum_{i=1}^{N_j}}{R}\left(\theta_{z,i^j}; \mu_\beta^j, \mu_w^j, \mu_\alpha^j\right). \tag{8}$$

As it was introduced in Section 2, the difference $\hat{\mu}^j_{R,0} - \mu^j_R$, hereinafter referred to as $\Delta^j_{R,0}$, is the underlying bias error at evaluating μ_R with the zero-order approximation for the j-th day. Likewise, the second-order approximation of daily mean solar radiation, $\hat{\mu}^j_{R,2}$, is calculated following Eq. (6) as:

$$\hat{\mu}^j_{R,2} = \hat{\mu}^j_{R,0} + \frac{1}{N_j}\sum_{i=1}^{N_j}\left[\frac{1}{2}\frac{\partial^2 R}{\partial \beta^2}\bigg|_{\Omega^j_i}\sigma^2_{\beta,j} + \frac{1}{2}\frac{\partial^2 R}{\partial w^2}\bigg|_{\Omega^j_i}\sigma^2_{w,j}\right], \tag{9}$$

where $\Omega^j_i = \left(\theta^j_{z,i};\, \mu^j_\beta, \mu^j_w, \mu^j_\alpha\right)$. As for the zero-order approximation, now $\Delta^j_{R,2} = \hat{\mu}^j_{R,2} - \mu^j_R$ is the error at evaluating μ_R with the second-order approximation for the j-th day. Note that the sub-daily variability in Eq. (8) and (9) is due only to solar zenith angle, $\theta^j_{z,i}$. The derivatives in Eq. (9) are evaluated using a third-order central-difference scheme.

4. Results and discussion

Fig. 3 shows the scatterplots of the actual GHI and DNI daily means μ^j_R *vis-á-vis* their zero-order approximation counterparts $\hat{\mu}^j_{R,0}$. The plots are presented by aerosol type. Overall, the discrepancies are lower for GHI than for DNI and for sites with prevailing coarse aerosol than prevailing fine aerosol.

The zero-order approximation error of GHI, $\Delta^j_{GHI,0}$, (Fig. 3a-c) stays nearly always within the typical expected GHI measurement error bounds (grayish area). The mean bias deviation stays reasonably similar regardless the prevailing aerosol type, with a combined value (i.e., including all sites) of -0.19 W/m^2 (see Table 1). For DNI, the zero-order approximation error, $\Delta^j_{DNI,0}$, (Fig. 3d-f) goes more often beyond the reference measurement error bounds, especially at fine aerosol sites, where site days with errors as high

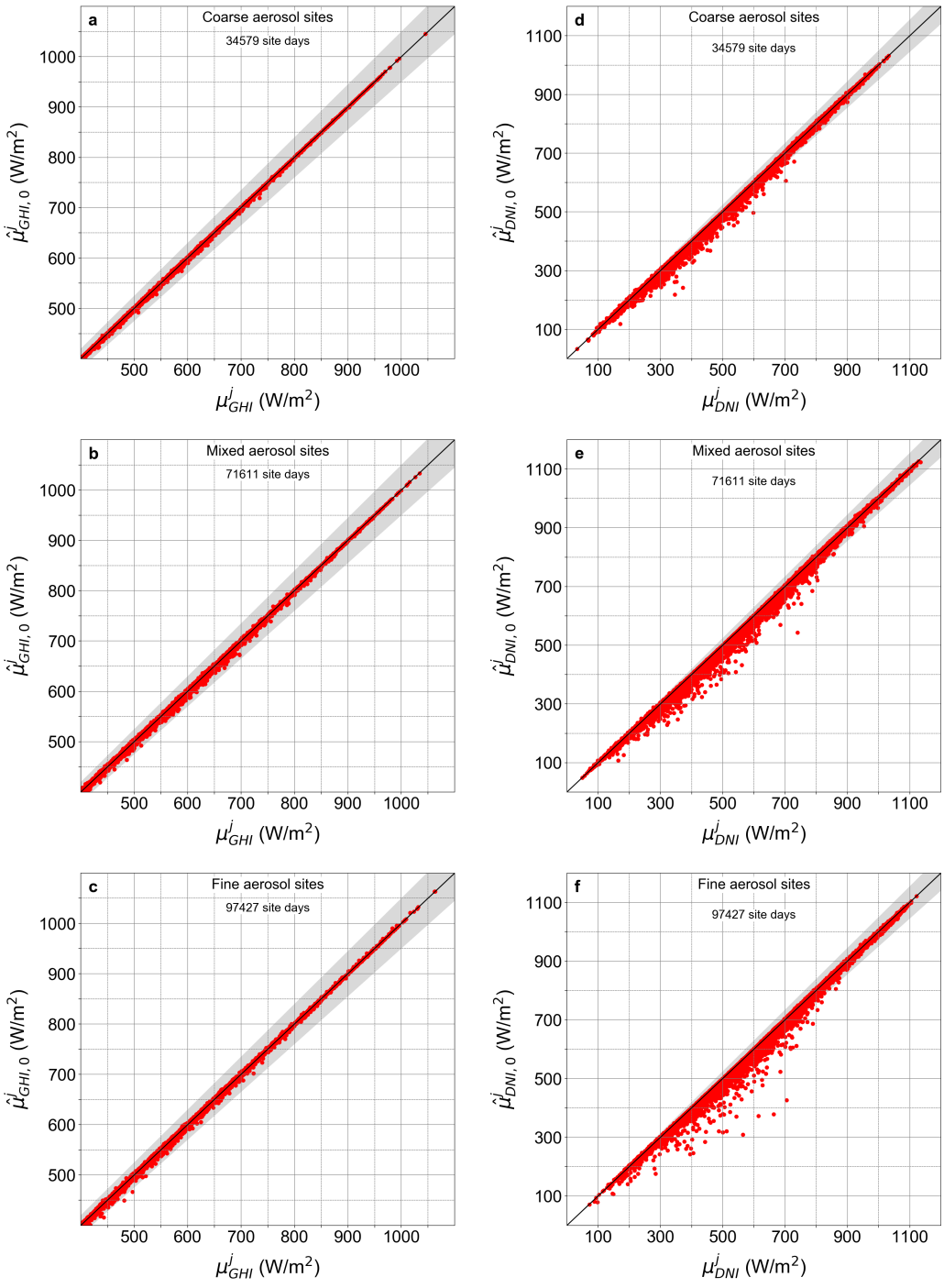

Figure 3: Scatterplots of μ^j_R *vs.* $\hat{\mu}^j_{R,0}$ for GHI (left column) and DNI (right column) for each aerosol type. The grayish area highlights the typically expected measurement error bounds of solar irradiance, taken here as 5 % following Habte et al. (2016).

as 200 W/m^2, or more, are shown. The mean bias deviation increases to nearly or above 2 W/m^2 in all aerosol types, and has a combined value of -1.95 W/m^2 (see Table 1). Overall, MBD for DNI is negative but with magnitude comparable to that of MAD meaning that the differences are most often negative as advanced in Section 2.

The right side of Table 1 shows that adding the second-order Taylor correction to the zero-order approximation diminishes the bias for both GHI and DNI and reduces the combined MAD from 0.69 W/m^2 to 0.61 W/m^2 for GHI (reduction of 12 %) and from 2.75 W/m^2 to 1.87 W/m^2 for DNI (reduction of 32 %). It shows also that 90 % of the $\Delta^j_{GHI,0}$ and $\Delta^j_{DNI,0}$ combined values stay below 1.54 W/m^2 and 5.91 W/m^2, respectively. However, these figures drop to 1.39 W/m^2 and 4.22 W/m^2 when the second-order approximation is used to compute the GHI and DNI daily means, respectively.

Fig. 4 shows the scatterplots of the actual GHI and DNI daily means *vis-á-vis* their second-order approximations, $\hat{\mu}^j_{R,2}$. Compared to Fig. 3, the second-order approximations stay more tightly clustered within the expected measurement error bounds (i.e., ± 5 %), especially at the coarse aerosol sites. The $\hat{\mu}^j_{R,2}$ values go beyond the expected measurement error bounds for very few days for GHI at mixed and fine aerosol sites and for few days for DNI, especially at the mixed and fine aerosol sites (markers highlighted with blue edges in Fig. 4). Note that these days involve only a tiny part of the entire observational dataset: 0.34 %, 0.24 % and 0.14 % of the site days for DNI at coarse, mixed and fine aerosol sites, respectively. These fractions contrast with the perception from Fig. 4 that departures from the expected measurement error bounds are more probable at fine aerosol sites. The violin

Table 1: Statistical scores of the zero- and second-order approximation errors of daily mean GHI and DNI. The column scores are: mean bias difference, MBD= $\frac{1}{N}\sum_j \Delta_R^j$; mean absolute difference, MAD= $\frac{1}{N}\sum_j |\Delta_R^j|$; standard deviation, STD= $\left[\frac{1}{N}\sum_j (\Delta_R^j - \text{MBD})^2\right]^{\frac{1}{2}}$; percentile 66 of $\{|\Delta_R^j|\}$ (P66); and percentile 90 of $\{|\Delta_R^j|\}$ (P90). All figures are in W/m^2.

	0th-order approximation				2nd-order approximation			
	MBD	MAD	STD	P90	MBD	MAD	STD	P90
GHI								
Coarse aerosol	−0.21	0.70	1.06	1.54	0.09	0.63	0.88	1.40
Mixed aerosol	−0.21	0.76	1.29	1.70	0.04	0.64	1.02	1.45
Fine aerosol	−0.17	0.63	1.07	1.43	0.12	0.58	1.04	1.34
All combined	−0.19	0.69	1.15	1.54	0.09	0.61	1.01	1.39
DNI								
Coarse aerosol	−2.03	2.83	5.17	6.22	0.01	1.78	2.75	4.12
Mixed aerosol	−1.87	2.87	5.52	6.07	0.00	2.11	3.45	4.75
Fine aerosol	−1.98	2.63	5.60	5.67	−0.05	1.72	3.28	3.84
All combined	−1.95	2.75	5.50	5.91	−0.02	1.87	3.26	4.22

plots of each panel in Fig. 4 depict the distributions of Δ_R^j for the zero- and second-order approximations. Clearly, the latter diminishes the bias (virtually removing it for DNI) and reduces the spread of residues compared to the zero-order approximation, consistently with the results already shown in Table 1.

To gain understanding on the reasons that lead to deviations of $\hat{\mu}_{DNI,2}^j$ beyond the expected measurement error bounds, Tables 2-4 show the mean prevailing conditions during the site days for which $|\Delta_{DNI,2}^j|$ is greater than 5 % and for which it is less or equal than 5 % for each aerosol type. Overall, both μ_β^j and $\sigma_{\beta,j}$ are notably higher in all cases when $|\Delta_{DNI,2}^j| > 5$ % which appears to indicate that the validity of the Taylor approximation under highly turbid and variable conditions may become questionable. Note that precisely highly turbid sites are typically characterized by highly variable aerosol turbidity (Ruiz-Arias et al., 2016a). The increase of the deviations of $\hat{\mu}_{DNI,2}^j$ is likely reinforced by higher μ_w^j and $\sigma_{w,j}$ values that overall also occur when $|\Delta_{DNI,2}^j| > 5$ % except for μ_w^j in coarse aerosol sites. With regards to Angström exponent, it appears that extreme situations such as low values at coarse aerosol sites and high values at fine aerosol sites, may also contribute to the increase of the magnitude of $\Delta_{DNI,2}^j$. However, they might just be a result of the high turbidity episodes included within the cases for which $|\Delta_{DNI,2}^j| > 5$ %, such as dust storms in coarse locations and pollution outbreaks in fine aerosol sites, but its verification would require further scrutiny that is out of the scope of this study. These conclusions, to a lower extent, also hold for GHI.

The Angström turbidity insets in Fig. 2b show that AOD at the coarse

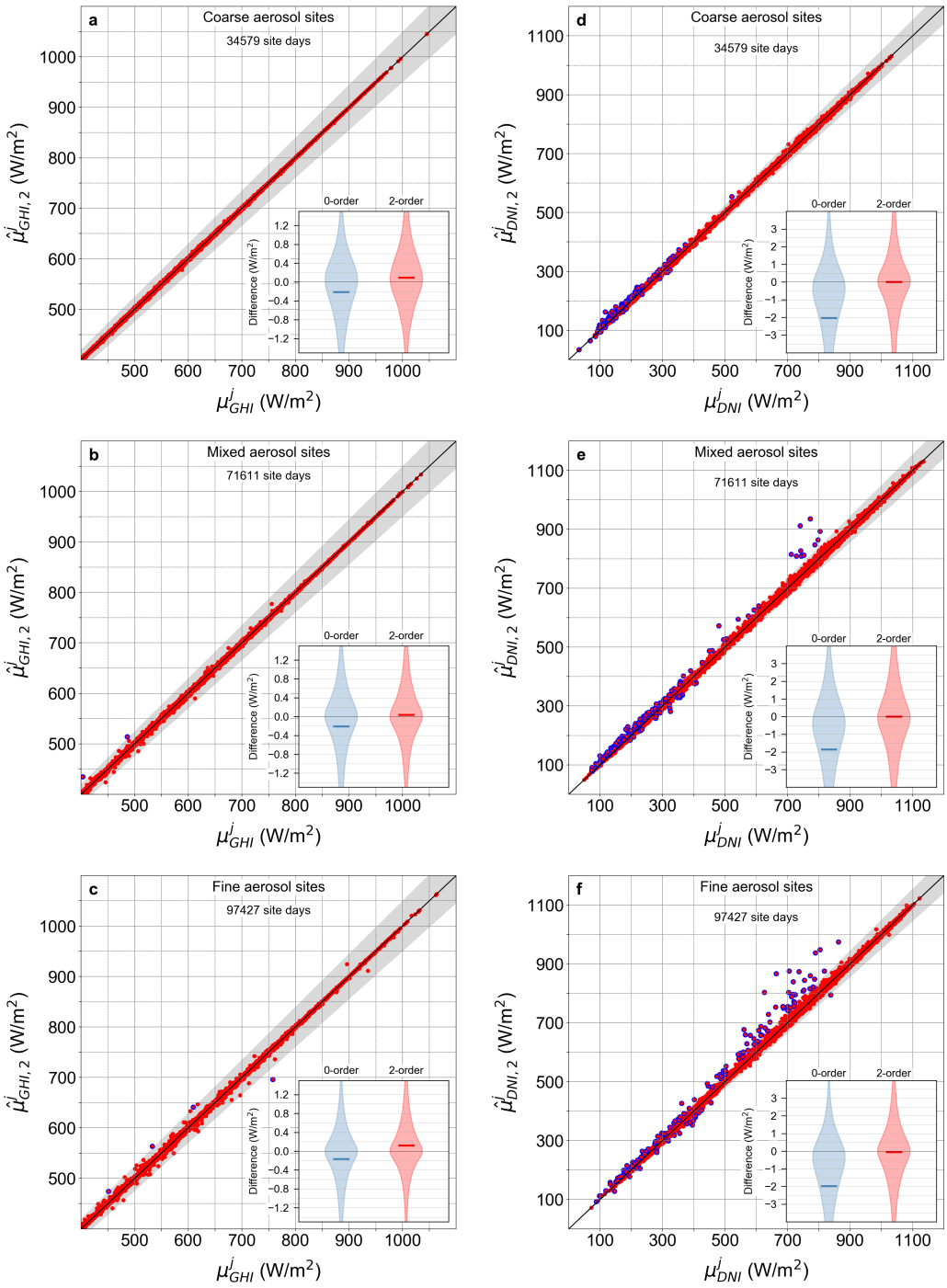

Figure 4: As Fig. 3 but for $\hat{\mu}^j_{R,2}$. The edge of the markers for site days beyond the expected measurement error bounds are highlighted in blue. The violin plots in each panel show the distribution of $\Delta^j_{R,0}$ and $\Delta^j_{R,2}$ in each case.

Table 2: Mean value of site day characteristics at the coarse aerosol sites for days with $|\Delta^j_{DNI,2}|$ greater than 5 % (blue-edged points in Fig. 4d) and less or equal than 5 % (rest of points in Fig. 4d). The columns are the mean of: number of daily counts (N_j), daily mean Angström turbidity (μ^j_β), daily standard deviation of Angström turbidity ($\sigma_{\beta,j}$), daily mean precipitable water (μ^j_w) in cm, daily standard deviation of precipitable water ($\sigma_{w,j}$) in cm, daily mean Angström exponent (μ^j_α), daily mean DNI (μ^j_{DNI}) in W/m^2, and magnitude of the daily mean DNI second-order approximation error, $|\Delta^j_{DNI,2}|$, in percent. The mean solar zenith angle is about 53° in both cases.

	N_j	μ^j_β	$\sigma_{\beta,j}$	μ^j_w	$\sigma_{w,j}$	μ^j_α	μ^j_{DNI}	$\lvert\Delta^j_{DNI,2}\rvert$
$\lvert\Delta^j_{DNI,2}\rvert > 5\%$	37.6	1.04	0.26	1.84	0.18	0.18	182	8.2
$\lvert\Delta^j_{DNI,2}\rvert \leq 5\%$	47.2	0.23	0.05	2.00	0.17	0.54	605	0.3

Table 3: As Table 2 but for sites with mixed aerosol type (data in Fig. 4e). The mean solar zenith angle is about 54° in both cases.

	N_j	μ^j_β	$\sigma_{\beta,j}$	μ^j_w	$\sigma_{w,j}$	μ^j_α	μ^j_{DNI}	$\lvert\Delta^j_{DNI,2}\rvert$
$\lvert\Delta^j_{DNI,2}\rvert > 5\%$	43.0	0.72	0.27	2.17	0.24	1.11	256	9.0
$\lvert\Delta^j_{DNI,2}\rvert \leq 5\%$	48.8	0.08	0.03	1.44	0.15	1.07	767	0.3

Table 4: As Table 2 but for sites with fine aerosol type (data in Fig. 4f). The mean solar zenith angle is about 56° in both cases.

	N_j	μ^j_β	$\sigma_{\beta,j}$	μ^j_w	$\sigma_{w,j}$	μ^j_α	μ^j_{DNI}	$\lvert\Delta^j_{DNI,2}\rvert$
$\lvert\Delta^j_{DNI,2}\rvert > 5\%$	57.9	0.42	0.29	1.98	0.22	1.65	428	8.9
$\lvert\Delta^j_{DNI,2}\rvert \leq 5\%$	55.1	0.06	0.02	1.53	0.15	1.43	770	0.2

aerosol sites is, overall, higher and more variable than at fine aerosol sites. Thus, it seems counterintuitive that the misalignments shown in Fig. 3 at the coarse aerosol sites appear smaller than at the fine aerosol sites, specially, for DNI. However, as it is expected, the magnitude of $\Delta^j_{DNI,0}$ values at the coarse sites in Table 1 is, at least, slightly greater than at the fine sites (-2.03 W/m^2 *vs.* -1.98 W/m^2, respectively). At first sight, Table 1 and Fig. 3 show contradictory results. A closer inspection of this issue, particularized for DNI, is presented in Fig. 5, which shows the distribution of observations in the space $(\mu^j_\beta, \sigma^2_{\beta,j})$ for coarse and fine aerosol sites. The 0.5 % of days with the highest $\Delta^j_{DNI,0}$ values are colored by error magnitude. They all fall within the space area with low or moderate turbidity and/or high intra daily variability. Overall, the days with high intra-daily variability at fine aerosol sites typically occur with coincidentally lower daily mean turbidities than at coarse aerosol sites and the highest $\Delta^j_{DNI,0}$ at the former are greater than at the latter, consistently with the misalignments seen in Fig. 3 at fine aerosol sites.

The fact that days with high intra-daily variability and high (low) turbidity result in relatively modest (important) Δ^j_R differences, typical situations at coarse (fine) aerosol sites, can be explained in virtue of Eq. (5). To that aim, one must note that the atmospheric transmittance by aerosols, which is a decaying exponential, becomes: 1) less sensitive to AOD changes at large AODs and, 2) more sensitive to AOD changes at low AODs as Angström exponent increases. This favors that the second derivative of the radiative transfer model with respect to AOD in the Taylor correction terms dominates over the intra-daily variability of AOD for situations with high turbidities

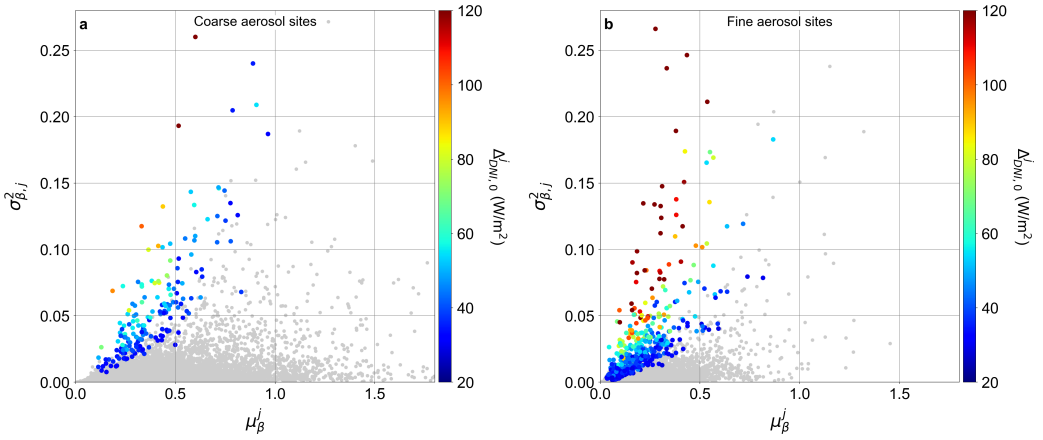

Figure 5: Distribution of observations in the space (μ^j_β, $\sigma^2_{\beta,j}$) for coarse (a) and fine (b) aerosol sites. The 0.5 % of days with the highest $\Delta^j_{DNI,0}$ are colored by error magnitude in W/m^2.

at coarse aerosol sites (small second derivative) and enhances the effect of high intra-daily variability of AOD for situations with low turbidities at fine aerosol sites (large second derivative).

5. Conclusions

The non-resolved intra-daily variability of AOD induces a systematic deviation in the calculations of the daily mean (or sum) of solar irradiance at the surface (both GHI and DNI) as compared to when AOD is fully resolved at sub-daily time scale. It has been shown that: 1) the deviation is caused by the non-linearity of the atmospheric radiative processes involving AOD and, 2) it is proportional to the intra-daily AOD variance. A data set of 213 AERONET sites roughly classified by prevailing aerosol type as coarse, mixed and fine has been used to evaluate such a systematic deviation. To that aim, the SMARTS radiative transfer model has been used to compute

GHI and DNI. Overall, the error in GHI stays very similar regardless the aerosol type at about -0.2 W/m^2 (all sites combined), with only 10 % of the samples featuring an error greater than about 1.5 W/m^2. For DNI, the error is nearly ten times higher (-1.95 W/m^2 at all sites combined) with 10 % of the samples featuring an error greater than nearly 6 W/m^2 at all sites combined.

Overall, the systematic error is slightly higher at coarse sites than at fine sites. However, the very highest errors at fine aerosol sites are (or can be) much higher than at coarse aerosol sites because, although the intra-daily AOD variance can be similar at both kinds of sites, the aerosol transmittance is more sensitive to AOD changes at low AODs and high Angström's exponents, typical situation at fine aerosol sites.

Overall, the results of this study suggest that the underlying bias in modeled GHI due to the use of daily rather than sub-daily aerosol properties and precipitable water may not be critical for most practical applications, in constrast with the modeled DNI in which the bias increases up to about 2 W/m^2. The mathematical framework presented here can be used to predict this systematic deviation just making use of aggregated variables of AOD (mean and variance) and, possibly, of other variables involved in the calculation of solar irradiance such as precipitable water. It can be likewise applied to other time scales, not necessarily restricted only to daily intervals.

In subsequent studies the role of other variables such as Angström exponent and the cross-correlations between all of them will be evaluated, as well as potential improvements based on the consideration of higher-order Taylor correction terms.

Acknowledgments

The author is indebted to the personnel of the AERONET network who kindly acquired, processed and shared publicly the aerosol optical depth and precipitable water data used in this study, which have been retrieved from *h*ttps://aeronet.gsfc.nasa.gov. The author is also grateful to Dr. Christian A. Gueymard for sharing the SMARTS radiative transfer model code, which has been instrumental to the success of this work.

References

Benedetti, A., Reid, J.S., Knippertz, P., Marsham, J.H., Giuseppe, F.D., Remy, S., Basart, S., Boucher, O., Brooks, I.M., Menut, L., et al., 2018. Status and future of numerical atmospheric aerosol prediction with a focus on data requirements. Atm. Chem. Phys 18, 10615–10643. doi:10.5194/acp-18-10615-2018.

Benedetti, A., Vitart, P., 2018. Can the direct effect of aerosols improve subseasonal predictability? Mon. Weather. Rev. 146, 3481–3498. doi:10.1175/MWR-D-17-0282.1.

Bohren, C.F., Clothiaux, E.E., 2006. Fundamentals of Atmospheric Radiation: An Introduction with 400 Problems. Wiley–CH, Weinheim, Germany.

Bozzo, A., Remy, S., Benedetti, A., Flemming, J., Bechtold, P., Rodwell, M., Morcrette, J.J., 2017. Implementation of a CAMS-based aerosol climatology in the IFS. Technical Report 801. ECMWF. Reading, UK. doi:10.21957/84ya94mls.

De Leeuw, G., Holzer-Popp, T., Bevan, S., Davies, W.H., Descloitres, J., Grainger, R.G., Griesfeller, J., Heckel, A., Kinne, S., Klüser, L., et al., 2015. Evaluation of seven European aerosol optical depth retrieval algorithms for climate analysis. Remote Sensing of Environment 162, 295–315. doi:10.1016/j.rse.2013.04.023.

Diner, D., Abdou, W., Bruegge, C., Conel, J., Crean, K., Gaitley, B., Helmlinger, M., Kahn, R., Martonchik, J., Pilorz, S., et al., 2001. MISR aerosol optical depth retrievals over southern Africa during the SAFARI-2000 dry season campaign. Geophys. Res. Lett. 28, 3127–3130. doi:10.1029/2001GL013188.

Eck, T.F., Holben, B.N., Reid, J.S., Dubovik, O., Smirnov, A., O'neill, N.T., Slutsker, I., Kinne, S., 1999. Wavelength dependence of the optical depth of biomass burning, urban, and desert dust aerosols. J. Geophys. Res.-Atmos. 104, 31333–31349. doi:10.1029/1999JD900923.

Gelaro, R., McCarty, W., Suárez, M.J., Todling, R., Molod, A., Takacs, L., Randles, C.A., Darmenov, A., Bosilovich, M.G., Reichle, R., et al., 2017. The Modern-Era Retrospective analysis for Research and Applications, Version 2 (MERRA-2). J. Climate 30, 5419–5454. doi:10.1175/JCLI-D-16-0758.1.

Giles, D.M., Sinyuk, A., Sorokin, M.G., Schafer, J.S., Smirnov, A., Slutsker, I., Eck, T.F., Holben, B.N., Lewis, J.R., Campbell, J.R., et al., 2019. Advancements in the Aerosol Robotic Network (AERONET) Version 3 database–automated near-real-time quality control algorithm with improved cloud screening for Sun photometer aerosol optical depth (AOD)

measurements. Atmos. Meas. Tech. 12, 169–209. doi:10.5194/amt-12-169-2019.

Gueymard, C.A., 2019. The SMARTS spectral irradiance model after 25 years: New developments and validation of reference spectra. Sol. Energy 187, 233–253. doi:10.1016/j.solener.2019.05.048.

Gueymard, C.A., Sengupta, M., 2013. Improved gridded aerosol data for India. Technical Report NREL/TP-5D00-58762. National Renewable Energy Laboratory(NREL). Golden, CO. URL: https://www.nrel.gov/docs/fy14osti/58762.pdf.

Habte, A., Sengupta, M., Andreas, A., Wilcox, S., Stoffel, T., 2016. Intercomparison of 51 radiometers for determining global horizontal irradiance and direct normal irradiance measurements. Sol. Energy 133, 372–393. doi:10.1016/j.solener.2016.03.065.

Hinkelman, L.M., 2019. The Global Radiative Energy Budget in MERRA and MERRA-2: Evaluation with Respect to CERES EBAF Data. J. Climate 32, 1973–1994. doi:10.1175/JCLI-D-18-0445.1.

Inness, A., Ades, M., Agusti-Panareda, A., Barré, J., Benedictow, A., Blechschmidt, A.M., Dominguez, J.J., Engelen, R., Eskes, H., Flemming, J., et al., 2019. The CAMS reanalysis of atmospheric composition. Atm. Chem. Phys 19, 3515–3556. doi:10.5194/acp-19-3515-2019.

Kaufman, Y.J., Holben, B.N., Tanré, D., Slutsker, I., Smirnov, A., Eck, T.F., 2000. Will aerosol measurements from Terra and Aqua polar orbit-

ing satellites represent the daily aerosol abundance and properties? Geophys. Res. Lett. 27, 3861–3864. doi:10.1029/2000GL011968.

Kinne, S., O'Donnel, D., Stier, P., Kloster, S., Zhang, K., Schmidt, H., Rast, S., Giorgetta, M., Eck, T.F., Stevens, B., 2013. MAC-v1: A new global aerosol climatology for climate studies. J. Adv. Model. Earth Sys. 5, 704–740. doi:10.1002/jame.20035.

Kocha, C., Tulet, P., Lafore, J.P., Flamant, C., 2013. The importance of the diurnal cycle of Aerosol Optical Depth in West Africa. Geophys. Res. Lett. 40, 785–790. doi:10.1002/grl.50143.

Levy, R., Mattoo, S., Munchak, L., Remer, L., Sayer, A., Patadia, F., Hsu, N., 2013. The Collection 6 MODIS aerosol products over land and ocean. Atmos. Meas. Tech. 6, 2989. doi:10.5194/amt-6-2989-2013.

Levy, R.C., Leptoukh, G.G., Kahn, R., Zubko, V., Gopalan, A., Remer, L.A., 2009. A critical look at deriving monthly aerosol optical depth from satellite data. IEEE T. Geosci. Remote 47, 2942–2956. doi:10.1109/TGRS.2009.2013842.

Levy, R.C., Remer, L.A., Mattoo, S., Vermote, E.F., Kaufman, Y.J., 2007. Second-generation operational algorithm: Retrieval of aerosol properties over land from inversion of Moderate Resolution Imaging Spectroradiometer spectral reflectance. J. Geophys. Res.-Atmos. 112. doi:10.1029/2006JD007815.

Ruiz-Arias, J.A., Dudhia, J., Gueymard, C.A., Pozo-Vázquez, D., 2013a. Assessment of the Level-3 MODIS daily aerosol optical depth in the context of

surface solar radiation and numerical weather modeling. Atm. Chem. Phys 13, 675–692. doi:10.5194/acp-13-675-2013.

Ruiz-Arias, J.A., Dudhia, J., Lara-Fanego, V., Pozo-Vázquez, D., 2013b. A geostatistical approach for producing daily Level-3 MODIS aerosol optical depth analyses. Atmos. Environ. 79, 395–405. doi:10.1016/j.atmosenv.2013.07.002.

Ruiz-Arias, J.A., Dudhia, J., Santos-Alamillos, F.J., Pozo-Vázquez, D., 2013c. Surface clear-sky shortwave radiative closure intercomparisons in the Weather Research and Forecasting model. J. Geophys. Res.-Atmos. 118, 9901–9913. doi:10.1002/jgrd.50778.

Ruiz-Arias, J.A., Gueymard, C.A., 2018a. A multi-model benchmarking of direct and global clear-sky solar irradiance predictions at arid sites using a reference physical radiative transfer model. Sol. Energy 171, 447–465. doi:10.1016/j.solener.2018.06.048.

Ruiz-Arias, J.A., Gueymard, C.A., 2018b. Worldwide inter-comparison of clear-sky solar radiation models: Consensus-based review of direct and global irradiance components simulated at the earth surface. Sol. Energy 168, 10–29. doi:10.1016/j.solener.2018.02.008.

Ruiz-Arias, J.A., Gueymard, C.A., Quesada-Ruiz, S., Santos-Alamillos, F.J., Pozo-Vázquez, D., 2016a. Bias induced by the AOD representation time scale in long-term solar radiation calculations. Part 1: Sensitivity of the AOD distribution to the representation time scale. Sol. Energy 137, 608–620. doi:10.1016/j.solener.2016.06.026.

513 Ruiz-Arias, J.A., Gueymard, C.A., Santos-Alamillos, F.J., Pozo-Vázquez,
514 D., 2016b. Worldwide impact of aerosol's time scale on the predicted
515 long-term concentrating solar power potential. Sci. Rep. 6, 30546.
516 doi:10.1038/srep30546.

517 Ruiz-Arias, J.A., Gueymard, C.A., Santos-Alamillos, F.J., Quesada-Ruiz,
518 S., Pozo-Vázquez, D., 2016c. Bias induced by the AOD representa-
519 tion time scale in long-term solar radiation calculations. Part 2: Im-
520 pact on long-term solar irradiance predictions. Sol. Energy 135, 625–632.
521 doi:10.1016/j.solener.2016.06.017.

522 Schulz, M., Kinne, S., 2009. The Aerosol Model Comparison Project, Ae-
523 roCom, Phase II: Clearing Up Diversity, in: IGAC Newsletter. 41. URL:
524 https://aerocom.met.no/pdfs/May_2009_IGAC_41.pdf.

525 Smirnov, A., Holben, B., Eck, T., Slutsker, I., Chatenet, B., Pinker,
526 R., 2002. Diurnal variability of aerosol optical depth observed at
527 AERONET (Aerosol Robotic Network) sites. Geophys. Res. Lett. 29, 30–1.
528 doi:10.1029/2002GL016305.

529 Wild, M., Folini, D., Hakuba, M.Z., Schär, C., Seneviratne, S.I., Kato, S.,
530 Rutan, D., Ammann, C., Wood, E.F., König-Langlo, G., 2015. The en-
531 ergy balance over land and oceans: an assessment based on direct ob-
532 servations and CMIP5 climate models. Clim. Dynam. 44, 3393–3429.
533 doi:10.1007/s00382-014-2430-z.

534 Yang, J., Hu, M., 2018. Filling the missing data gaps of daily MODIS AOD

using spatiotemporal interpolation. Science of the Total Environment 633, 677–683. doi:10.1016/j.scitotenv.2018.03.202.

Zubler, E., Lohmann, U., Lüthi, D., Schär, C., 2011. Intercomparison of aerosol climatologies for use in a regional climate model over Europe. Geophys. Res. Lett. 38. doi:10.1029/2011GL048081.